■ **Electrochemistry**

A Combined "Electrochemical–Frustrated Lewis Pair" Approach to Hydrogen Activation: Surface Catalytic Effects at Platinum Electrodes

Elliot J. Lawrence,[a] Robin J. Blagg,[a] David L. Hughes,[a] Andrew E. Ashley,[b] and Gregory G. Wildgoose*[a]

Abstract: Herein, we extend our "combined electrochemical–frustrated Lewis pair" approach to include Pt electrode surfaces for the first time. We found that the voltammetric response of an electrochemical–frustrated Lewis pair (FLP) system involving the $B(C_6F_5)_3$/$[HB(C_6F_5)_3]^-$ redox couple exhibits a strong surface electrocatalytic effect at Pt electrodes. Using a combination of kinetic competition studies in the presence of a H atom scavenger, 6-bromohexene, and by changing the steric bulk of the Lewis acid borane catalyst from $B(C_6F_5)_3$ to $B(C_6Cl_5)_3$, the mechanism of electrochemical–FLP reactions on Pt surfaces was shown to be dominated by hydrogen-atom transfer (HAT) between Pt, [Pt–H] adatoms and transient $[HB(C_6F_5)_3]^{\cdot}$ electrooxidation intermediates. These findings provide further insight into this new area of combining electrochemical and FLP reactions, and proffers additional avenues for exploration beyond energy generation, such as in electrosynthesis.

Introduction

The field of frustrated Lewis pair (FLP) chemistry has continued to grow rapidly since the pioneering work of Stephan's group in 2006.[1] The combination of suitably sterically encumbered Lewis acid and Lewis base (LB) components (that are incapable of forming classical Lewis adducts) were found to heterolytically cleave H_2, resulting in hydridic and protic components. Whilst the inception of FLPs is relatively recent, Brown and co-workers first uncovered the concept of steric frustration in 1942, when they failed to form a Lewis adduct from the combination of lutidine and BMe_3.[2] The application of FLPs for the activation of H_2 and other small molecules has been reviewed extensively.[3–6] For main-group FLPs, the Lewis acid component is typically based on electron-deficient boranes, typically $B(C_6F_5)_3$ and its derivatives,[1,7–10] although FLP H_2 activation has also been achieved by using analogous $Al(C_6F_5)_3$[11] and boranes that do not contain C_6F_5 groups.[12–17] FLPs are not limited to

the main group;[18–20] Wass and co-workers previously demonstrated the ability of zirconocene–phosphinoaryloxide complexes to mimic the reactivity of FLPs and offer additional, unprecedented reactivity towards small molecules.[19]

The majority of literature reports focus on delivering the resulting hydride to reduce a wide range of functional groups including imines, enamines and nitriles;[21–23] aldehydes;[8] and activate small molecules, such as CO_2.[24–26]

We have recently introduced a new approach to H_2 oxidation by combining FLP chemistry to heterolytically cleave H_2 with in situ electrochemical oxidation of the resultant borohydride.[27,28] Through combining Stephan's archetypal $B(C_6F_5)_3$ (**1**)/tBu_3P FLP with the electrochemical oxidation of the generated $[HB(C_6F_5)_3]^-$, [**1**-H]$^-$, the voltage required for H_2 oxidation at a glassy carbon electrode (GCE) was found to be reduced by 610 mV (equivalent to a reduction in the required energetic driving force of 177.7 kJ mol^{-1}). The digital simulation of voltammetric data combined with chemical mechanistic studies and DFT calculations allowed us to propose that the oxidation of [**1**-H]$^-$ follows the mechanism at carbon electrode surfaces as shown in Scheme 1.

This concept holds great promise for precious metal-free energy-generation applications, such as fuel-cell technologies, in which extensive research efforts into aqueous-phase borohydride, $[BH_4]^-$ electrooxidation at Pt electrodes have already been invested.[29–33] Aside from our recent studies using carbon electrodes, the non-aqueous redox chemistry of bulkier borohydrides, such as [**1**-H]$^-$,[27,34] and their parent electron-deficient, Lewis acidic boranes,[35,36] remain largely unexplored. Therefore, to better understand the oxidation mechanism of important intermediates, such as [**1**-H]$^-$ in combined electro-

[a] *E. J. Lawrence, Dr. R. J. Blagg, Dr. D. L. Hughes, Dr. G. G. Wildgoose*
Energy Materials Laboratory
School of Chemistry, University of East Anglia
Norwich Research Park, Norwich, NR4 7TJ (UK)
E-mail: g.wildgoose@uea.ac.uk

[b] *Dr. A. E. Ashley*
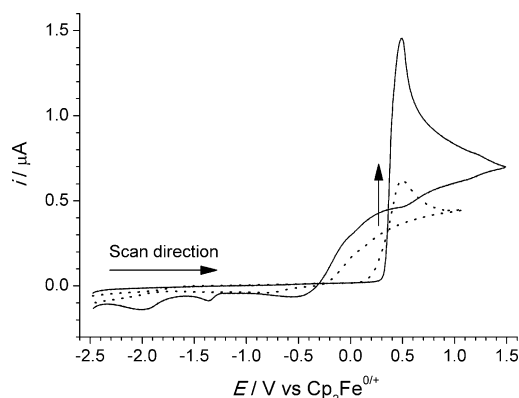*Department of Chemistry, Imperial College London*
South Kensington, London, SW7 2AZ (UK)
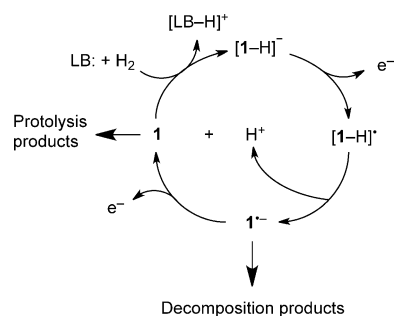
Scheme 1. Proposed redox mechanism for the oxidation of [1-H]⁻ at a glassy carbon electrode surface (LB = Lewis base).[27]

Figure 2. Comparison of the voltammetry for a 5 mM solution of [nBu$_4$N][1-H] recorded at Pt (dashed line) and glassy carbon (solid line) macrodisk electrodes in CH$_2$Cl$_2$, containing 0.05 M [nBu$_4$N][B(C$_6$F$_5$)$_4$] electrolyte, at a scan rate of 100 mV s⁻¹. Note that the current density, j, is plotted to allow a direct comparison between electrodes of different geometric areas.

chemical–FLP systems, herein, we seek to explore and understand the electrochemical behaviour of [1-H]⁻ at Pt electrode surfaces.
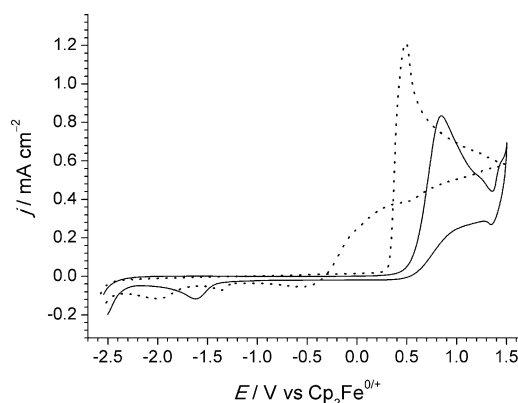
Results and Discussion

The oxidative redox chemistry of an authentic sample of [nBu$_4$N][1-H] at 2.3 mM and 4.8 mM concentrations in CH$_2$Cl$_2$ solutions containing 0.05 M [nBu$_4$N][B(C$_6$F$_5$)$_4$] as a weakly coordinating electrolyte[36] was explored at a Pt macrodisk electrode by using cyclic voltammetry (Figure 1). When the poten-

Figure 1. Cyclic voltammetry of [nBu$_4$N][1-H] at a Pt macrodisk electrode (2.3 mM; dashed line; and 4.8 mM (solid line); 0.05 M [nBu$_4$N][B(C$_6$F$_5$)$_4$], CH$_2$Cl$_2$) recorded at a scan rate of 100 mV s⁻¹.

tial was swept in a positive direction, a large, well-defined oxidative wave was observed at +0.49 V versus Cp$_2$Fe$^{0/+}$. The potential scan direction was reversed just before the limit of the solvent potential window, in which the current was observed to cross-over the forward-going current, and remained positive (indicating an oxidation was occurring) at potentials more negative than the oxidation potential of [1-H]⁻. The current then gradually decreased (whilst still remaining positive) until it recrossed the forward scan in the region of −0.30 to −0.25 V versus Cp$_2$Fe$^{0/+}$; a series of small, ill-defined reduction waves were observed at more negative potentials.

The observed voltammetric response at a Pt macrodisk electrode is in stark contrast to what has been observed previously
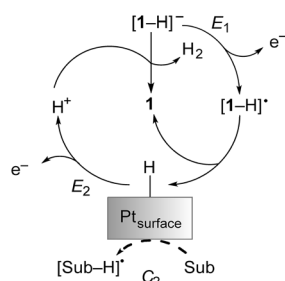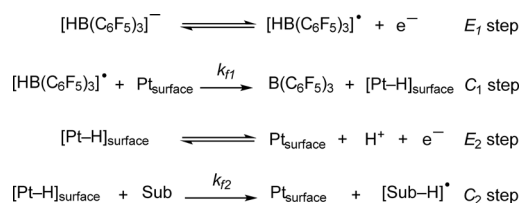
at a GCE (Figure 2), in which a more typical electrochemically reversible, but chemically irreversible oxidation wave was observed with no observable corresponding reduction wave, no current-crossing and a small reduction wave at a more negative potential assigned to the reduction of the parent B(C$_6$F$_5$)$_3$, 1.[27,36] The observation of a crossing current in cyclic voltammetry is unusual; for an oxidation process, this signifies the formation of a new electroactive product that has a much lower reduction potential. This effect is only observed in either special cases of a homogenous ECE-type mechanism,[37] or when a change in the electrode surface structure occurs, usually during an electrocatalytic process for example, significant current-crossover is observed when methanol is oxidized at Pt electrodes, owing to the formation of various adsorbed intermediate species that are electroactive at lower oxidation potentials.[38] In our case, the height at which the reverse current crosses the forward-going current strongly suggests that the latter scenario, a surface change on the electrode, is likely responsible for this effect.

It is clear from these results that the Pt electrode is non-innocent and exhibits strong electrocatalytic properties. For example, the rate of electron transfer during the oxidation of [1-H]⁻ is very much faster at the Pt electrode than at the GCE, leading to a much steeper gradient in the rising part of the oxidation wave, a sharper peak, and an overall larger peak current density recorded at the Pt electrode (Figure 2). Furthermore, the oxidative peak current is shifted by −390 mV at Pt compared to the GCE—evidence of strong surface electrocatalysis.

To explain these phenomena, we propose a modification to our earlier mechanism for the oxidation of [1-H]⁻ on a GCE[27] that takes into account the well-documented ability of Pt surfaces to adsorb H atoms, as is observed in the direct, electrocatalytic oxidation of H$_2$ at Pt electrodes in aqueous electrolytes (Scheme 2).[39,40] The initial step, the one-electron oxidation of [1-H]⁻, occurs at both Pt and GCE to form a transient [HB(C$_6$F$_5$)$_3$]⁻ radical, [1-H]⁻. DFT calculations showed that the SOMO of [1-H]⁻ is somewhat delocalised over the aryl rings;

$$[HB(C_6F_5)_3]^- \; \rightleftharpoons \; [HB(C_6F_5)_3]^\bullet + e^- \qquad E_1 \text{ step}$$

$$[HB(C_6F_5)_3]^\bullet + Pt_{surface} \xrightarrow{k_{f1}} B(C_6F_5)_3 + [Pt-H]_{surface} \qquad C_1 \text{ step}$$

$$[Pt-H]_{surface} \; \rightleftharpoons \; Pt_{surface} + H^+ + e^- \qquad E_2 \text{ step}$$

$$[Pt-H]_{surface} + Sub \xrightarrow{k_{f2}} Pt_{surface} + [Sub-H]^\bullet \qquad C_2 \text{ step}$$

Scheme 2. Proposed redox mechanism with individual steps for the electro-catalytic oxidation of [1-H]⁻ at a Pt electrode surface (labelled in Testa–Reinmuth notation, top) and the schematic representation of the entire mechanistic cycle (bottom). The decomposition pathways of **1** and **1**˙⁻ are omitted for clarity (see Scheme 1 and text for details). Also shown is the competing hydrogen atom transfer reaction, labelled as C₂, between a substrate, Sub, and the [Pt-H]ₛᵤᵣfₐcₑ species.

however, the majority of spin density is located in the B—H bond, which is significantly weakened, with a bond enthalpy of approximately 30 kJ mol⁻¹.[27] At carbon electrodes, this radical dissociates very rapidly to form a proton and a **1**˙⁻ radical anion, which undergoes further oxidation in competition with its decomposition in solution (Scheme 1). However, the Pt electrode surface is able to compete effectively with the dissociation step and abstracts a hydrogen atom from [1-H]˙, liberating the parent borane, **1**, and forming a H adatom on the surface of the electrode, Pt—H. This hydrogen-atom transfer (HAT) reaction effects a change on the surface of the electrode. Because the oxidation potential of Pt—H is very much less than the potential at this point in the cyclic voltammogram (close to the oxidation peak potential observed), it rapidly undergoes a second one-electron oxidation to form a proton and regenerate the Pt active site on the electrode in an electrocatalytic fashion. This process is occurring throughout the beginning of the reverse sweep, such that there is a significant surface concentration of Pt—H at the potential, in which the current crosses-over the forward-going scan, and this continues to be oxidized, giving rise to an oxidative current at potentials more negative than that of the oxidation of [1-H]⁻, until the potential approaches the reduction potential of the Pt—H system around −0.3 V versus Cp₂Fe⁰/⁺, in which the current decreases, and the reverse reaction, reduction of protons to form Pt—H, occurs at the electrode surface.

Note that all electron transfer steps are reversible, and therefore subject to Nernstian equilibrium.[37] Perturbation of the surface concentration of [1-H]˙ by competition with Pt—H formation is responsible for the reduction in the apparent oxidation potential of [1-H]⁻ at Pt versus GCE, and explains why the onset of oxidation occurs on Pt at less positive potentials than

at glassy carbon, that is, is electrocatalytic at Pt. With reference to our earlier work,[27,36] we assign the small reduction wave at approximately −2.0 V versus Cp₂Fe⁰/⁺ to the reduction of **1**. Note that we have shown that this arises mainly by the reaction of incoming [1-H]⁻ reacting with electrogenerated protons, hence, why the reduction peak is small in comparison to the oxidation peak; most of the electrogenerated **1** undergoes protolytic decomposition.[27] Proton reduction on the polycrystalline Pt surface in CH₂Cl₂ may also be responsible for the small, ill-defined reduction waves seen between approximately −0.3 and −2.0 V, an assignment supported by the observation of similar voltammetric features when CH₂Cl₂ is spiked with the oxonium acid, [H(OEt₂)₂][B(C₆F₅)₄].[41]

The change on the surface of the electrode unfortunately prevented us from attempting digital simulation of the voltammetric data, to extract the relevant kinetic and thermodynamic parameters and to confirm the proposed mechanism by fitting the experimental data. Nonetheless, evidence to support our proposed mechanism was obtained by: 1) competition experiments with an hydrogen atom scavenger; 2) increasing the steric bulk surrounding the B—H bond by replacing C₆F₅ groups with C₆Cl₅ groups as [HB(C₆Cl₅)₃]⁻, [2-H]⁻.

To investigate our proposed mechanism we conducted cyclic voltammetry of [1-H]⁻ in the presence of increasing molar equivalents of 6-bromo-1-hexene. This known radical clock acts as a scavenger for H atoms, forming 5-hexenyl radical intermediates that cyclize at a known rate[42–48] and was chosen as neither the parent radical clock nor any of the intermediate radicals or cyclized products have any redox chemistry in the potential window of interest. Figure 3 shows the cyclic
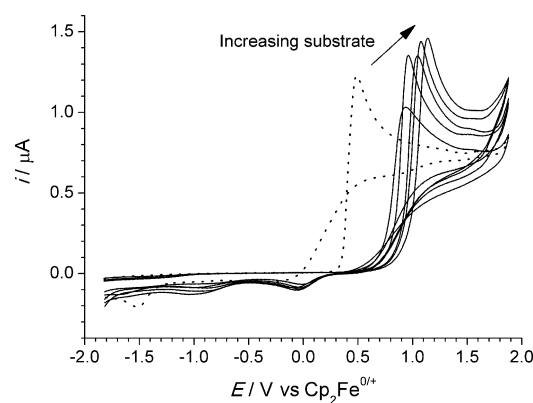
Figure 3. Overlaid cyclic voltammograms of a 4.8 mM solution of [nBu₄N][1-H] (dotted line) with increasing addition of 6-bromo-1-hexene (black lines; from left to right: 1, 2, 4, 8, and 10 equiv) recorded at a Pt macrodisk electrode in CH₂Cl₂ containing 0.05 M [nBu₄N][B(C₆F₅)₄] electrolyte at a voltage scan rate of 100 mV s⁻¹.

voltammograms recorded for the oxidation of [1-H]⁻ in the presence of 0–10 molar equivalents of the radical clock.

Upon the addition of a first molar equivalent of radical clock, the oxidation wave of [1-H]⁻ shifts to more positive potentials, decreases in height, and crucially, does not exhibit any current cross-over effects. Indeed, the voltammetry is very similar to that observed at a bare GCE both in terms of peak po-

tential, wave shape and peak current. This can be understood in terms of the radical clock competing very effectively with the Pt electrode surface to abstract a hydrogen atom from the transient [**1**-H]· species, thus preventing the formation of Pt–H on the surface. Thus, the catalytic oxidation step for the Pt–H surface species at reduced potentials (Scheme 2) is "switched-off" and the oxidation mechanism of [**1**-H]⁻ now occurs along the same reaction pathway as it does at the GCE electrode (Scheme 1). Thus, the H atom scavenger 6-bromo-1-hexene acts as a competitive inhibitor for any surface electrocatalytic step by the Pt electrode. When the concentration of radical clock is increased, the peak potential gradually increases as does the peak current. The increase in peak potential is a direct effect of the reaction between 6-bromo-1-hexene and [**1**-H]·, which perturbs the Nernstian equilibrium governing the initial oxidation of [**1**-H]⁻, thereby increasing the peak potential. The increase in peak current can be understood in similar terms: the abstraction of a H atom from [**1**-H]· prevents its dissociation into protons, and therefore inhibits the reaction of protons with a second incoming [**1**-H]⁻ (see Scheme 1), which would otherwise lead to a decrease in the observed oxidation current.

Another synthetic route to inhibit the formation of Pt–H surface adatom formation is to increase the steric bulk around the B–H bond, and thus sterically "shield" the hydrogen atom from any interaction with the Pt electrode surface. Our approach required the synthesis of the hitherto unknown borohydride, [nBu_4N][$HB(C_6Cl_5)_3$], [nBu_4N][**2**-H], by treating the parent perchlorinated analogue of **1**, $B(C_6Cl_5)_3$ (**2**), with Na[$HBEt_3$] in toluene at 80 °C, and then metathesizing the resulting Na⁺ cation with [nBu_4N]⁺ to impart the required solubility for non-aqueous electrochemistry. Note that this Lewis acidic borane was chosen, because we have previously reported the synthesis and voltammetric characterization of **2**,[35] which is a much more electron-deficient borane than **1** (despite Cl being less electronegative than F, the Hammet parameter at the para ring position of Cl is greater (σ_{para}(Cl) 0.227; σ_{para}(F) 0.062) as a result of weaker (3p–2p) π overlap with the aromatic ring), and that the $-C_6Cl_5$ substituents have a greater steric profile than $-C_6F_5$ (see Figure 4 for a comparison of the space-filling models of [**1**-H]⁻ and [**2**-H]⁻).

Cyclic voltammetry of [**2**-H]⁻ indicates that it is oxidized at a slightly higher potential (ca. 100 mV) than [**1**-H]⁻, suggesting that [**2**-H]⁻ is less hydridic than [**1**-H]⁻ (Figure 5). This is consistent with the parent borane, **2**, being more electrophilic than **1**.[35] However, in the case of [**2**-H]⁻, no current cross-over was observed at any scan rate, indicating that the steric bulk around the B–H bond in [**2**-H]⁻ is sufficient to prevent the formation of any Pt–H surface species, and thus any electrocatalysis by the electrode surface, and lends further support for our proposed mechanism for the electrocatalytic oxidation of [**1**-H]⁻ in Scheme 2. Instead a new, quasi-reversible redox wave was observed at a mid-peak potential of +0.98 mV versus $Cp_2Fe^{0/+}$. Noting that the height of the first oxidation wave corresponds to a single-electron oxidation, and that in the parent Lewis acid, **2**, the central boron atom is sufficiently sterically shielded that its radical anion, formed upon electroreduc-
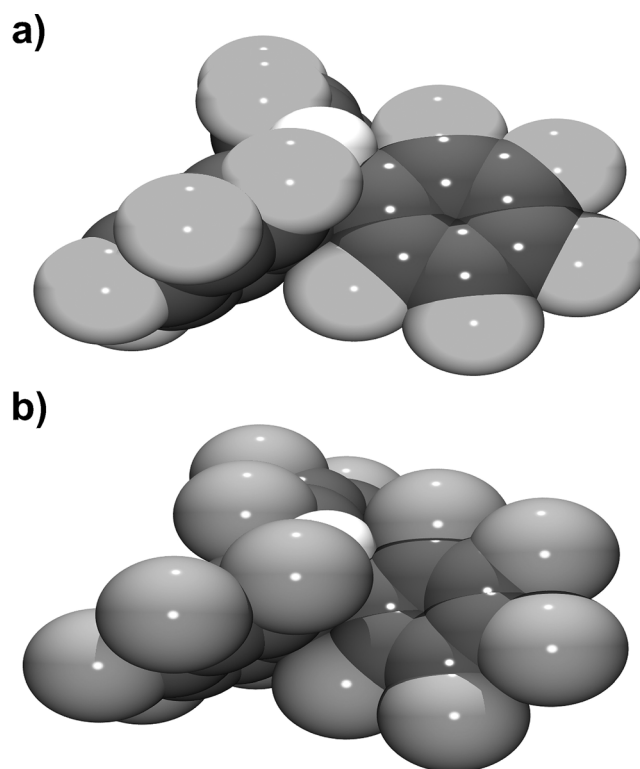
Figure 4. Space-filling view of the ions of a) [**1**-H]⁻ and b) [**2**-H]⁻, showing the extent of steric shielding of the B–H bond by the surrounding C_6Cl_5 groups. Only the major components of disordered groups are shown.
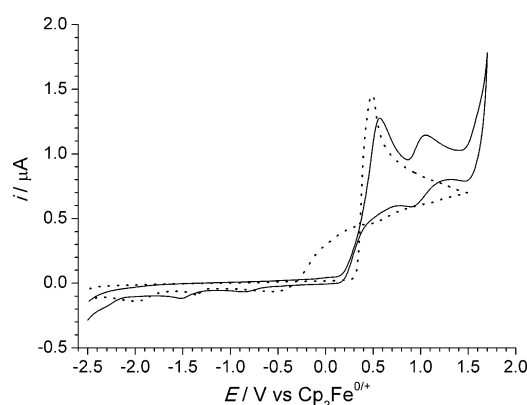
Figure 5. Overlaid cyclic voltammetry comparing the oxidation of 5.0 mM solutions of [**1**-H]⁻ (dashed line) and [**2**-H]⁻ (solid line) at a Pt macrodisk electrode (0.05 M [nBu_4N][$B(C_6F_5)_4$], CH_2Cl_2, scan rate 100 mV s⁻¹).

tion, is stable in solution (unlike that of **1**), we tentatively propose that this voltammetric feature corresponds to the one-electron oxidation of [**2**-H]· radicals, which are relatively long-lived intermediates in contrast to [**1**-H]·, and which occurs alongside competing solvolysis/dissociation steps. Whether this is indeed due to an identifiable B–H bonded species or whether free H· is dissociatively formed in a "cage" within the void formed by the central B atom and neighbouring aryl–Cl groups, and possibly the solvent, is the subject of ongoing investigations. What is clear is that this new voltammetric feature only arises as a result of the increased steric bulk surrounding the central boron atom.
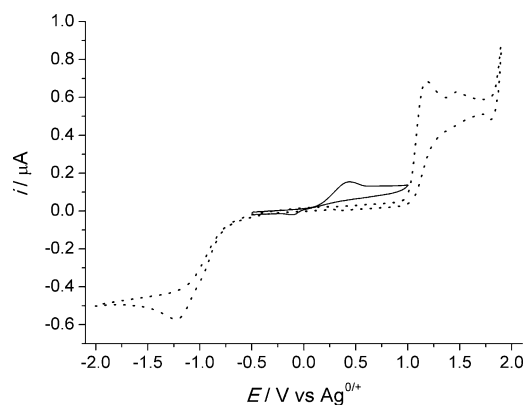
Figure 6. Overlaid cyclic voltammograms demonstrating the TMP/B(C_6F_5)$_3$ FLP system (5 mM equimolar solutions) before (dotted line) and after (solid line) a 1 h sparge with H$_2$ (0.05 M [nBu$_4$N][B(C_6F_5)$_4$], CH$_2$Cl$_2$ electrolyte, scan rate 100 mV s^{-1}).

Finally, for completeness, we examined the in situ combined electrochemical frustrated Lewis pair activation of H$_2$ at Pt, in much the same fashion as our previous efforts at a GCE. Figure 6 shows the voltammetry of a 1:1 solution of the FLP B(C_6F_5)$_3$/TMP (TMP = 2,2,6,6-tetramethylpiperidine, a frustrated Lewis base) at Pt whereupon the reduction of **1** and the oxidation of TMP are initially clearly observed under N$_2$ (dotted line, Figure 6). H$_2$ was bubbled through the electrolyte solution for a period of one hour, before a second cyclic voltammogram was recorded (solid line, Figure 6). Although the kinetics of H$_2$ cleavage by this FLP system are relatively slow, even after one hour of sparging with H$_2$, clear voltammetric evidence for the formation of [**1**-H]$^-$ was observed as a new peak at +0.43 V versus Ag$^{0/+}$, intermediate between the oxidation of TMP and the reduction of **1**. Although this new peak is broadened compared with an authentic sample of [**1**-H]$^-$ due to its low concentration, it is characteristic of the voltammetry of [**1**-H]$^-$, and evidence for the in situ combined electrochemical frustrated Lewis pair activation of H$_2$. Whilst this result is less applicable to energy applications, in which one would directly oxidize H$_2$ in aqueous electrolyte at Pt, in light of our findings above, it does open up the tantalizing prospect of using combined electrochemical frustrated Lewis pair chemistry to electrocatalytically activate H$_2$ for HAT reactions with potential applications in novel electrosynthesis. This prospect forms part of our ongoing collaborative research efforts to further develop our combined electrochemical–frustrated Lewis pair approach.

Conclusion

We have investigated the hitherto unexplored electrochemistry of bulky borohydrides, namely, the tris(pentafluorophenyl)borohydride anion and its perchlorinated analogue, at Pt electrode surfaces. We have found that the Pt electrode exhibits strong electrocatalytic properties within the electrochemical–FLP system. Evidence of strong surface-based electrocatalysis was given by a significant current crossover (surface change) in the cyclic voltammetry of authentic [**1**-H]$^-$ and, more importantly, a 390 mV reduction in the oxidation peak potential

compared to GCE materials. The electrocatalytic effect of Pt, which involves HAT reactions, was "switched off" in the presence of a competing radical scavenger. In addition, this electrocatalysis was not observed when [**1**-H]$^-$ was substituted for a relatively bulky perchlorinated analogue, [**2**-H]$^-$. The use of platinum electrodes in conjunction with combined electrochemical–FLP systems permit a significant energy saving for the effective conversion of chemical energy, stored in the H—H bond, to electrical energy that is available for work. The elucidated electrochemical mechanism suggests the prospect of using combined electrochemical frustrated Lewis pair chemistry to activate H$_2$ for HAT reactions. This opens up a completely new area for exploration for the combined electrochemical–frustrated Lewis pair concept, with potential applications in electrosynthetic catalysis.

Experimental Section

General

All synthetic reactions and manipulations were performed under a dry N$_2$ atmosphere (BOC Gases) by using standard Schlenk-line techniques on a dual manifold vacuum/inert gas line or either a Saffron or MBraun glovebox. All glassware was flame-dried under vacuum before use. Anhydrous solvents were dried by refluxing over appropriate drying agents: molten Na for toluene, CaH$_2$ for dichloromethane; and collected via distillation. All solvents were sparged with nitrogen gas to remove any trace of dissolved oxygen and stored in ampules over activated 4 Å molecular sieves. Na[HBEt$_3$] (1.0 M in toluene) was purchased from Sigma–Aldrich and used without further purification. nBu$_4$NCl was purchased from Alfa Aesar and recrystallized from anhydrous acetone prior to use. Hydrogen gas (99.995%) was purchased from BOC gases and passed over drying columns containing P$_4$O$_{10}$ and 4 Å molecular sieves prior to use. Deuterated NMR solvents ([D$_6$]DMSO, 99.9%; CDCl$_3$, 99.8%) were purchased from Cambridge Isotope Laboratories Inc. and were dried over P$_4$O$_{10}$, degassed using a triple freeze/pump/thaw cycle and stored over activated 4 Å molecular sieves. Compounds [nBu$_4$N][**1**-H],[27] **1**,[49] **2**,[35] [nBu$_4$N][B(C_6F_5)$_4$],[50] and tBu$_3$P[51] were prepared according to literature methods. NMR spectra were recorded by using either a Bruker Avance DPX-300 or DPX-500 MHz spectrometers. Chemical shifts are reported in ppm and are referenced relative to appropriate standards; ^{11}B is relative to Et$_2$O·BF$_3$, ^{31}P is relative to 85% H$_3$PO$_4$.

Electrochemistry

All electrochemical experiments were performed by using either an Autolab PGSTAT 30 or PGSTAT 302N computer-controlled potentiostat (Utrecht, The Netherlands). Cyclic voltammetry (CV) was performed by using a three-electrode configuration consisting of either a glassy carbon macrodisk working electrode (GCE; diameter of 3 mm; BASi, Indiana, USA) or a Pt macrodisk working electrode (diameter of 0.4 mm, 99.99%; GoodFellow, Cambridge, UK), combined with a Pt wire counter electrode (99.99%; GoodFellow, Cambridge, UK) and a Ag wire pseudo-reference electrode (99.99%; GoodFellow, Cambridge, UK). The GCE was polished between experiments using successive grades of diamond paste slurries from 3.0 to 0.1 μm (Kemet, Maidstone, UK). The Pt working electrodes were polished between experiments using 0.3 μm α-alumina slurry in distilled water. The electrodes were briefly sonicated in distilled water and rinsed with ethanol (GCE) or distilled water (Pt) between

each polishing step, to remove any adhered microparticles. The electrodes were then dried in an oven at 100 °C to remove any residual traces of water. The Pt and GCE electroactive area was calibrated for each experiment using a 5 mM ferrocene solution in CH_3CN solvent containing 0.1 M $[nBu_4N][PF_6]$ as the supporting electrolyte. The electroactive area was accurately determined by construction of a Randles–Sevcik plot from cyclic voltammograms recorded at varying scan rates (50–750 mVs^{-1}).[37] The Ag wire pseudo-reference electrodes were calibrated to the ferrocene/ferrocenium couple in CH_2Cl_2 at the end of each run to allow for any drift in potential, following IUPAC recommendations.[52] All electrochemical measurements were performed at ambient temperatures under an inert N_2 atmosphere in CH_2Cl_2 containing 0.05 M $[nBu_4N][B(C_6F_5)_4]$ as the supporting electrolyte. All electrochemical measurements were iR compensated to within 80±5% of the solution uncompensated resistance.

Synthesis of Na[HB(C_6Cl_5)$_3$], Na[2-H]

A clear colourless solution of 1.0 M Na[HBEt$_3$] in toluene (0.3 mL, 0.30 mmol) was added to a pale yellow suspension of B(C_6Cl_5)$_3$ (0.15 g, 0.20 mmol) in dry toluene (10 mL). The reaction mixture was heated to 80 °C and left to stir under N_2 overnight; warming resulted in dissolution of the suspension to give a pale yellow solution and a white precipitate formed as the reaction progressed. The reaction mixture was allowed to cool, and the precipitate was left to settle, before it was filtered and triturated with dry toluene (2×3 mL). The residue was dried in vacuo to yield Na[2-H] (0.14 g, 0.18 mmol) as a white powder in 89% yield. ^{1}H NMR (300 MHz, [D$_6$]DMSO, 25 °C, TMS): $\delta = 4.28$ ppm (br m, 1H; BH); ^{11}B NMR (96.3 MHz, [D$_6$]DMSO, 25 °C, BF$_3$.OEt$_2$): $\delta = -8.42$ ppm (br).

Synthesis of [nBu_4N][HB(C_6Cl_5)$_3$], [nBu_4N][2-H]

A clear colourless solution of nBu_4NCl (0.041 g, 0.15 mmol) in dry CH_2Cl_2 (3 mL) was added to a white suspension of Na[2-H] (0.12 g, 0.16 mmol) in dry CH_2Cl_2 (3 mL) at room temperature, with stirring under N_2. This resulted in the formation of a fine flocculent precipitate with the simultaneous breakup of the suspended material. The reaction mixture was left to stir overnight. The precipitate was then allowed to settle before it was filtered; the residue was triturated with dry CH_2Cl_2 (2×1.5 mL). The filtrate and extracts were combined and concentrated in vacuo to give [nBu_4N][2-H] (0.11 g, 0.11 mmol) as a white powder in 77% yield. Crystals suitable for X-ray crystallography (colourless needles) were grown by dissolving [nBu_4N][2-H] in a minimum quantity of dry CH_2Cl_2, warming to approximately 40 °C, adding an equal quantity of dry light petroleum ether and slow cooling to RT. ^{1}H NMR (300 MHz, CDCl$_3$, 25 °C, TMS): $\delta = 4.32$ (br m, 1H; BH), 3.12 (m, 8H; CH$_2$), 1.57 (m, 8H; CH$_2$), 1.35 (m, 8H; CH$_2$), 0.94 ppm (t, ^3J(H,H) = 7.1 Hz, 12H; CH$_3$); ^{11}B NMR (96.3 MHz, CDCl$_3$, 25 °C, BF$_3$·OEt$_2$): $\delta = -8.68$ ppm (d, ^1J(B,H) = 76 Hz); ^{13}C NMR (75.5 MHz, CDCl$_3$, 25 °C, TMS): $\delta = 138.2$, 138.0, 130.0, 129.7, 127.8, 59.1, 24.1, 19.9, 13.8 ppm.

Acknowledgements

[1] G. C. Welch, R. R. S. Juan, J. D. Masuda, D. W. Stephan, *Science* **2006**, *314*, 1124–1126.
[2] H. C. Brown, H. I. Schlesinger, S. Z. Cardon, *J. Am. Chem. Soc.* **1942**, *64*, 325–329.
[3] D. W. Stephan, in *Comprehensive Inorganic Chemistry II*, 2nd ed., (Ed.: J. R. Poeppelmeier), Elsevier, Amsterdam, **2013**, pp. 1069–1103.
[4] D. W. Stephan, G. Erker, *Angew. Chem. Int. Ed.* **2010**, *49*, 46–76; *Angew. Chem.* **2010**, *122*, 50–81.
[5] D. W. Stephan, *Dalton Trans.* **2009**, 3129.
[6] *Catalysis Without Precious Metals* (Ed.: R. M. Bullock), Wiley, Weinheim, **2010**.
[7] D. Holschumacher, T. Bannenberg, C. G. Hrib, P. G. Jones, M. Tamm, *Angew. Chem. Int. Ed.* **2008**, *47*, 7428–7432; *Angew. Chem.* **2008**, *120*, 7538–7542.
[8] V. Sumerin, F. Schulz, M. Nieger, M. Leskelä, T. Repo, B. Rieger, *Angew. Chem. Int. Ed.* **2008**, *47*, 6001–6003; *Angew. Chem.* **2008**, *120*, 6090–6092.
[9] G. C. Welch, D. W. Stephan, *J. Am. Chem. Soc.* **2007**, *129*, 1880–1881.
[10] P. Spies, G. Erker, G. Kehr, K. Bergander, R. Fröhlich, S. Grimme, D. W. Stephan, *Chem. Commun.* **2007**, 5072.
[11] G. Ménard, D. W. Stephan, *Angew. Chem. Int. Ed.* **2012**, *51*, 8272–8275; *Angew. Chem.* **2012**, *124*, 8397–8400.
[12] T. J. Herrington, A. J. W. Thom, A. J. P. White, A. E. Ashley, *Dalton Trans.* **2012**, *41*, 9019.
[13] E. L. Kolychev, T. Bannenberg, M. Freytag, C. G. Daniliuc, P. G. Jones, M. Tamm, *Chem. Eur. J.* **2012**, *18*, 16938–16946.
[14] S. C. Binding, H. Zaher, F. M. Chadwick, D. O'Hare, *Dalton Trans.* **2012**, *41*, 9061–9066.
[15] Z. Lu, Z. Cheng, Z. Chen, L. Weng, Z. H. Li, H. Wang, *Angew. Chem. Int. Ed.* **2011**, *50*, 12227–12231; *Angew. Chem.* **2011**, *123*, 12435–12439.
[16] J. M. Farrell, J. A. Hatnean, D. W. Stephan, *J. Am. Chem. Soc.* **2012**, *134*, 15728–15731.
[17] A. L. Travis, S. C. Binding, H. Zaher, T. A. Q. Arnold, J.-C. Buffet, D. O'Hare, *Dalton Trans.* **2013**, *42*, 2431.
[18] G. Erker, *Dalton Trans.* **2011**, *40*, 7475–7483.
[19] A. M. Chapman, M. F. Haddow, D. F. Wass, *J. Am. Chem. Soc.* **2011**, *133*, 18463–18478.
[20] M. T. Whited, *Beilstein J. Org. Chem.* **2012**, *8*, 1554–1563.
[21] P. A. Chase, T. Jurca, D. W. Stephan, *Chem. Commun.* **2008**, 1701.
[22] D. W. Stephan, *Org. Biomol. Chem.* **2012**, *10*, 5740–5746.
[23] D. W. Stephan, S. Greenberg, T. W. Graham, P. Chase, J. J. Hastie, S. J. Geier, J. M. Farrell, C. C. Brown, Z. M. Heiden, G. C. Welch, *Inorg. Chem.* **2011**, *50*, 12338–12348.
[24] S. D. Tran, T. A. Tronic, W. Kaminsky, D. Michael Heinekey, J. M. Mayer, *Inorg. Chim. Acta* **2011**, *369*, 126–132.
[25] A. E. Ashley, A. L. Thompson, D. O'Hare, *Angew. Chem. Int. Ed.* **2009**, *48*, 9839–9843; *Angew. Chem.* **2009**, *121*, 10023–10027.
[26] C. M. Mömming, E. Otten, G. Kehr, R. Fröhlich, S. Grimme, D. W. Stephan, G. Erker, *Angew. Chem. Int. Ed.* **2009**, *48*, 6643–6646; *Angew. Chem.* **2009**, *121*, 6770–6773.
[27] E. J. Lawrence, V. S. Oganesyan, D. L. Hughes, A. E. Ashley, G. G. Wildgoose, *J. Am. Chem. Soc.* **2014**, *136*, 6031–6036.
[28] E. J. Lawrence, T. J. Herrington, A. E. Ashley, G. G. Wildgoose, *Angew. Chem. Int. Ed.* **2014**, *53*, 9922–9925.
[29] C. P. de Leon, F. C. Walsh, D. Pletcher, D. J. Browning, J. B. Lakeman, *J. Power Sources* **2006**, *155*, 172–181.
[30] B. H. Liu, Z. P. Li, *J. Power Sources* **2009**, *187*, 291–297.
[31] J. Ma, N. A. Choudhury, Y. Sahai, *Renewable Sustainable Energy Rev.* **2010**, *14*, 183–199.
[32] D. M. F. Santos, C. A. C. Sequeira, *Renewable Sustainable Energy Rev.* **2011**, *15*, 3980–4001.
[33] I. Merino-Jiménez, C. Ponce de León, A. A. Shah, F. C. Walsh, *J. Power Sources* **2012**, *219*, 339–357.
[34] E. J. Lawrence, T. J. Herrington, A. E. Ashley, G. G. Wildgoose, *Angew. Chem. Int. Ed.* **2014**, DOI 10.1002/anie.201405721R1.

[35] A. E. Ashley, T. J. Herrington, G. G. Wildgoose, H. Zaher, A. L. Thompson, N. H. Rees, T. Krämer, D. O'Hare, *J. Am. Chem. Soc.* **2011**, *133*, 14727–14740.

[36] E. J. Lawrence, V. S. Oganesyan, G. G. Wildgoose, A. E. Ashley, *Dalton Trans.* **2013**, *42*, 782–789.

[37] R. G. Compton, C. E. Banks, *Understanding Voltammetry*, Imperial College Press, London, **2011**.

[38] T. Iwasita, *Electrochim. Acta* **2002**, *47*, 3663–3674.

[39] M. J. Croissant, T. Napporn, J.-M. Léger, C. Lamy, *Electrochim. Acta* **1998**, *43*, 2447–2457.

[40] T. Zhang, A. B. Anderson, *J. Phys. Chem. C* **2007**, *111*, 8644–8648.

[41] P. Jutzi, C. Müller, A. Stammler, H.-G. Stammler, *Organometallics* **2000**, *19*, 1442–1444.

[42] D. Griller, K. U. Ingold, *Acc. Chem. Res.* **1980**, *13*, 317–323.

[43] C. Chatgilialoglu, K. U. Ingold, J. C. Scaiano, *J. Am. Chem. Soc.* **1981**, *103*, 7739–7742.

[44] S. U. Pedersen, T. Lund, *Acta. Chem. Scand.* **1991**, *45*, 397–402.

[45] P. Cauliez, M. Benaskar, A. Ghanimi, J. Simonet, *New J. Chem.* **1998**, *22*, 253–261.

[46] E. Duñach, A. P. Esteves, A. M. Freitas, M. J. Medeiros, S. Olivero, *Tetrahedron Lett.* **1999**, *40*, 8693–8696.

[47] D. M. Fang, D. G. Peters, M. S. Mubarak, *J. Electrochem. Soc.* **2001**, *148*, E464–E467.

[48] A. P. Esteves, A. M. Freitas, M. J. Medeiros, D. Pletcher, *J. Electroanal. Chem.* **2001**, *499*, 95–102.

[49] S. J. Lancaster, *ChemSpider SyntheticPages* **2003**, DOI: 10.1039/SP215.

[50] R. J. LeSuer, C. Buttolph, W. E. Geiger, *Anal. Chem.* **2004**, *76*, 6395–6401.

[51] R. C. Srivastava, *J. Chem. Res. (S)* **1985**, *330*–331.

[52] G. Gritzner, J. Kůta, *Electrochim. Acta* **1984**, *29*, 869–873.